International Journal of Applied Earth Observation and Geoinformation 34 (2015) 78–88

Contents lists available at ScienceDirect

International Journal of Applied Earth Observation and Geoinformation

journal homepage: www.elsevier.com/locate/jag

Waveform-based point cloud classification in land-cover identification

Yi-Hsing Tseng, Cheng-Kai Wang, Hone-Jay Chu*, Yu-Chia Hung

Department of Geomatics, National Cheng Kung University, No. 1, University Road, Tainan City 701, Taiwan

ARTICLE INFO

Article history:
Received 24 April 2014
Accepted 18 July 2014
Available online 12 August 2014

Keywords:
Airborne LiDAR
Full-waveform topographic LiDAR
Waveform feature
Optical image
Point cloud classification
Waveform-based classifiers

ABSTRACT

Full-waveform topographic LiDAR data provide more detailed information about objects along the path of a laser pulse than discrete-return (echo) topographic LiDAR data. Full-waveform topographic LiDAR data consist of a succession of cross-section profiles of landscapes and each waveform can be decomposed into a sum of echoes. The echo number reveals critical information in classifying land cover types. Most land covers contain one echo, whereas topographic LiDAR data in trees and roof edges contained multi-echo waveform features. To identify land-cover types, waveform-based classifier was integrated single-echo and multi-echo classifiers for point cloud classification.

The experimental area was the Namasha district of Southern Taiwan, and the land-cover objects were categorized as roads, trees (canopy), grass (grass and crop), bare (bare ground), and buildings (buildings and roof edges). Waveform features were analyzed with respect to the single- and multi-echo laser-path samples, and the critical waveform features were selected according to the Bhattacharyya distance. Next, waveform-based classifiers were performed using support vector machine (SVM) with the local, spatial features of waveform topographic LiDAR information, and optical image information. Results showed that by using fused waveform and optical information, the waveform-based classifiers achieved the highest overall accuracy in identifying land-cover point clouds among the models, especially when compared to an echo-based classifier.

Introduction

Airborne laser scanning (ALS) data (also called topographic LiDAR data for *Light Detection and Ranging* data) are being used increasingly to classify land use and land cover (Wagner et al., 2008; Alexander et al., 2010; Heinzel and Koch, 2011; Crosilla et al., 2013; Dalponte et al., 2008). ALS systems apply two distinct techniques in which the return signal that is recorded is either full-waveform or discrete-return (also called multiple-return) (Alexander et al., 2010). Traditional discrete-return systems provide individual return with only discrete time measurements (Mallet et al., 2011). Full-waveform LiDAR data, which furnish more object information in the path of the laser pulse than discrete-return LiDAR data, consist of a succession of cross-section profiles of the landscape. Based on the waveform-based data, we can easily identify vertical profile of 3D object in the laser-pulse path when compared to only using echo-based (discrete-return) data.

The waveform pattern is affected by the surface reflectance, geometric structure, and roughness of the laser footprint. Amplitude, echo width, cross section, and the number of echoes (returns) are valuable parts of the information obtained from full-waveform data, which have been used successfully to classify land use and land cover (Alexander et al., 2010). For example, whereas echo amplitudes vary with the radiometric and geometric properties of targets, echo widths describe the durations of the received signal and can be applied easily in classification. Because the echoes for fields of trees are generally wider than those for roads or meadows (Wagner et al., 2008), echo width provides critical information for identifying vegetation types and detecting roads (Mallet et al., 2011; Hollaus et al., 2011). From the distance between the sensor and the target and from the amplitude and the width of an echo, the backscatter cross section can be derived, which is suitable for describing the scattering properties of targets (Alexander et al., 2010). Alexander et al. (2010) used major features such as the cross section in the classifier to distinguish between grass and roads successfully. Moreover, Crosilla et al. (2013) analyzed the skewness

* Corresponding author. Tel.: +886 6 2757575x63827; fax: +886 6 2375764.
E-mail addresses: honejay@mail.ncku.edu.tw, honejaychu@gmail.com (H.-J. Chu).

http://dx.doi.org/10.1016/j.jag.2014.07.004
1569-8432/

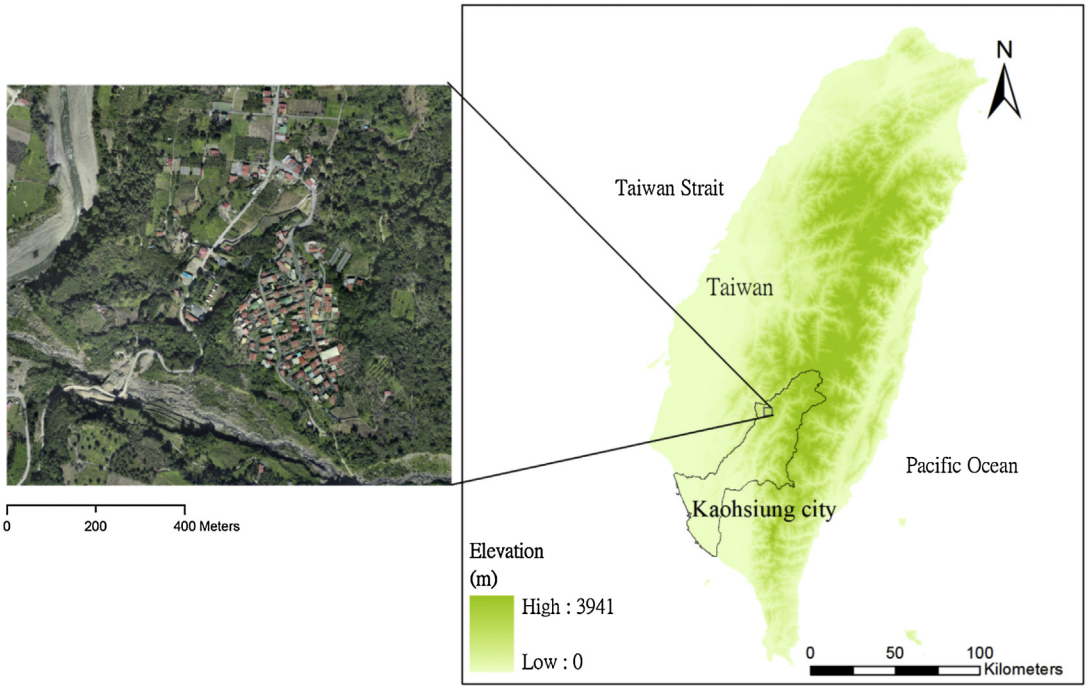

Fig. 1. Location of study area in Kaohsiung city of Taiwan.

and kurtosis of elevation and intensity-distribution values from LiDAR data for classification.

The extracted full-waveform features can be used for classifying land cover, especially for distinguishing vegetation from other land cover types. The first echo is often acquired from the vegetation and other surface features that can be penetrated, such as the crown and trunk of trees. The last echo is a return message indicating that the last laser pulse signal is attenuating to the end, which may contain ground information or non-ground points such as dense vegetation. Jutzi and Stilla (2003) showed that vegetation and roof edges contain features that generate multiple echoes, and thus echo numbers provide key information for classifying land cover. Therefore, LiDAR waveform information on land-cover types contains single-echo (number of echoes = 1) and multi-echo (number of echoes > 1) waveform features. To consider land cover with single-echo and multi-echo waveform features along the path of a laser pulse, waveform-based classifiers were applied that included both single-echo and multi-echo features in our current study.

LiDAR features also exhibit spatial autocorrelation, which indicates that the features in a sampling point are similar to those in a neighboring sampling point. The spatial (neighborhood) information on the features of each waveform is determined using the local waveform sets included in the cylindrical neighborhood centered on that waveform (Guo et al., 2011). In the study, the average or standard deviation of the waveform characteristics was selected in the neighborhood of each waveform as the spatial features in the classifier. Furthermore, LiDAR and optical image data are generally complementary (Guo et al., 2011; Mutlu et al., 2008). Multi-source data composed of full-waveform LiDAR data and orthoimages were used for point cloud classification. The orthoimage is composed of three spectral bands in the visible domain: Red (R), Green (G), and Blue (B). The RGB channels of an orthoimage are used as three independent optical features at the nearest locations of first-echo LiDAR points in this study.

Since waveform data can be divided into two categories, one contains single major echo such as the return waveforms from open ground. The other contains multiple echoes such as the return waveforms for trees and roof edges. Waveform features were analyzed with respect to the single- and multi-echo laser-path samples to investigate whether full-waveform data can provide effective information on land-cover classifications. In this study, waveform-based classifiers were performed using support vector machine (SVM) with the waveform LiDAR features, optical image information and the spatial features of LiDAR data. Finally, the classification accuracy of the waveform-based model was compared using the conventional echo-based classifier.

Study area and materials

Our study area was Namasha (Namaxia), which is a famous source of precious wood in Taiwan. Namasha is a suburban district in the northeastern part of Kaohsiung City that is located upstream from the Kao-ping river watershed (Fig. 1). Namasha suffered substantial destruction during Typhoon Morakot in 2009. The entire study area was 0.95 km^2, and the average elevation above the sea level and slope were approximately 722 m and 18°. Full-waveform LiDAR data were acquired from three LiDAR systems: Leica ALS60, Riegl LMS-Q680i, and Optech ALTM PEGASUS HD400. Three kinds of LiDAR data were used to prove the robustness of the

Table 1
Description of LiDAR data from Leica, Riegl and Optech systems.

Sensor	Leica ALS60	Riegl LMS-Q680i	Optech ALTM PEGASUS HD400
Wavelength (nm)	1064	1550	1064
Pulse rate (kHz)	55	220	150
Scan rate (Hz)	61	200	35
Field-of-view, FOV (degree)	6	60	40
Observation date	2011/10/30	2012/01/08	2011/10/07
Flight height (m)	2900	1900	2000
Beam divergence (mrad)	0.22	0.5	0.2
Footprint size (m)	0.64	0.95	0.4
Echo width (ns)	5	4	7
Point density (pts/m^2)	4.2	2.1	1.8

proposed classifiers. Table 1 lists the parameters of the topographic LiDAR systems. The waveform datasets were collected from Southern Taiwan in October 2011 and January 2012 by several fights. The strip sides overlapped more than 50% and the point densities of the study area were approximately 4.2, 2.1, and 1.8 points/m^2 in the Leica, Riegl, and Optech systems, respectively. The systems have laser-beam divergence angles of 0.22, 0.5 and 0.2 mrad on a target at nadir from a flying height of 2.9, 1.9 and 2 km, and produce approximately 0.64, 0.95, and 0.40 m footprint diameters in Leica, Riegl, and Optech systems. The radiometric correction each LiDAR system has been determined (Höfle and Pfeifer, 2007). In addition, the IGI DigiCAM is equipped with the Riegl LMS-Q680i system, to produce an orthoimage (the resolution of orthoimage is 0.25 m). GPS and IMU (inertial measurement unit) were used to acquire the position and attitude information of sensors. The LiDAR systems yielded horizontal accuracy of less than 0.40 m and vertical accuracy of less than 0.10 m.

Methods

Fig. 2 presents a flowchart of the proposed model in this study, which comprised data processing, feature selection, and classification. First, LiDAR waveforms were decomposed into waveform components. LiDAR features can be derived from the waveform components. According to the number of echoes of a waveform, the features can be generated and categorized as single-echo features (number of echoes = 1) and multi-echo features (number of echoes >1). Major features were then selected using the criterion of Bhattacharyya distance (Choi and Lee, 2003) for classifying. Our proposed classifying model for land-cover classification is to combine two classifiers, namely single-echo classifier and multi-echo classifier, which are designed according to the single-echo features and multi-echo features respectively. The proposed waveform-based classifying model is then used to compare with using echo-based classifier.The 3D point clouds were classified into five classes, namely, roads, trees (canopy), grass (grass and crop), bare (bare ground), and buildings (buildings and roof edges), based on the basic classifying model (echo-based) and our proposed classifying model. The details of the models were seen in Section "Classification models".

Data processing

The waveforms received can be composed of several echoes, and an echo-detection method is applied to the waveforms to identify the exact echoes present. In this study, a wavelet-based echo detector (Wang, 2012) was used that has been demonstrated to resolve overlapping echoes effectively and to also suppress noise. After the number of echoes and the echoes' positions were determined, a mixed-Gaussian curve was used to fit the waveform also known as the Gaussian decomposition (Wagner et al., 2006). With this decomposition method, each echo is represented by a

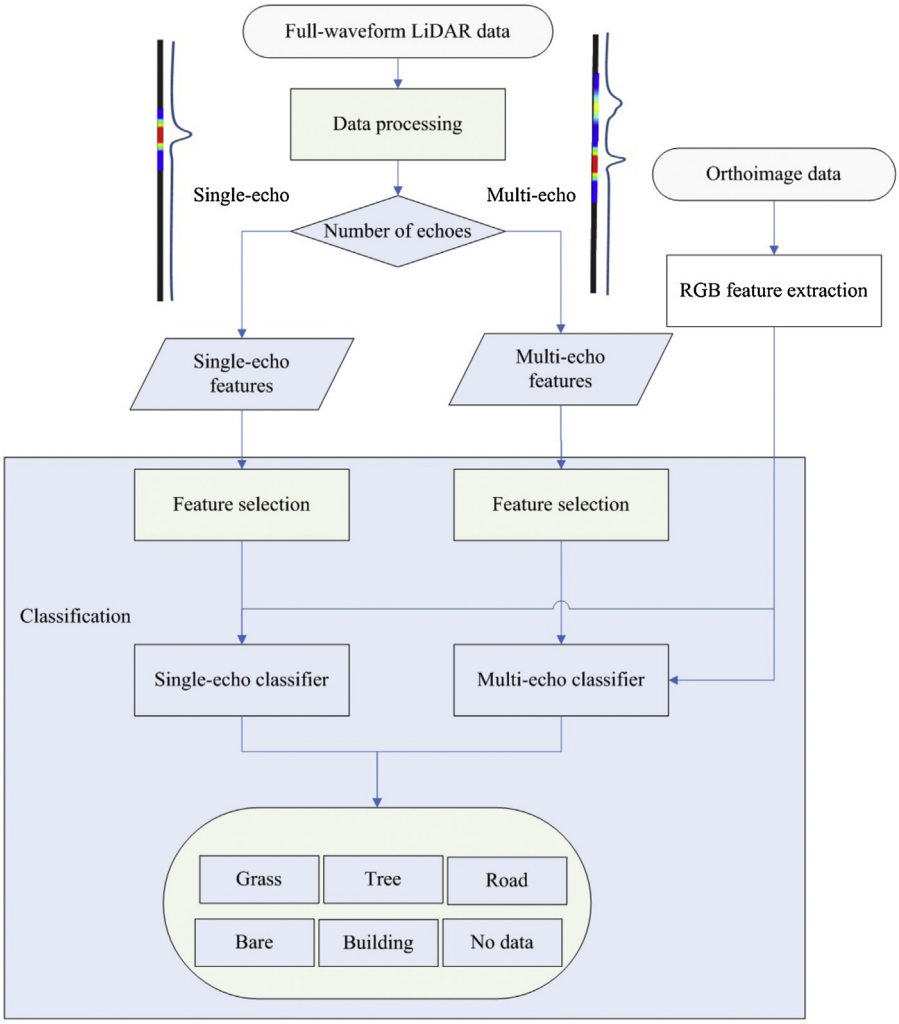

Fig. 2. Flowchart of waveform-based point cloud classifiers (model 3).

Table 2
Lists of LiDAR features including symbol name, symbol for average and symbol for standard deviation.

	Symbol	Name	Symbol for average[a]	Symbol for standard deviation[a]
Individual echo feature	Am	Echo amplitude	Avg Am	Std Am
	W	Echo width	Avg *W*	Std *W*
	A	Echo area	Avg *A*	Std *A*
	CS	Backscatter cross section	Avg CS	Std CS
	Sk	Echo skewness	–	–
	Kur	Echo kurtosis	–	–
	NR	Number of returns/echoes	Avg NR	Std NR
Multi echo feature	ΔAm	Amplitude difference of first and last echoes	Avg ΔAm	Std ΔAm
	Δ*W*	Width difference of first and last echoes	Avg Δ*W*	Std Δ*W*
	Δ*A*	Echo area difference of first and last echoes	Avg Δ*A*	Std Δ*A*
	ΔCS	Cross-section difference of first and last echoes	Avg ΔCS	Std ΔCS
	Δ*t*	Time from first to last echoes	Avg Δ*t*	Std Δ*t*
	OA	Overlap area of first and second echoes	Avg OA	Std OA
	OW	Overlap width of first and second echoes	Avg OW	Std OW

[a] The average and standard deviation of the feature information are exacted from a cylindrical neighborhood (radius is 4 m) of each waveform.

Gaussian function and the echo corresponding to the sensed object is characterized. Each echo can be then mapped into 3D point with the waveform features attached. Waveform features are then applied to the classification in this research.

Single-echo and multi-echo features

Waveform features can be divided into two categories: single-echo features and multi-echo features. The single-echo features describe each independent echo which can be obtained from either single return waveforms or echo-based waveforms. The multi-echo features describe the relation between echoes which can only be derived from waveforms that have two or more echoes. Table 2 lists the waveform features utilized and analyzed in this study. The single-echo features include echo amplitude (Am), echo width (*W*), echo area (*A*), backscatter cross section (CS), echo skewness (Sk), echo kurtosis (Kur). The multi-echo features include number of return (NR), amplitude difference of first and last echoes (ΔAm), width difference of first and last echoes (Δ*W*), echo area difference of first and last echoes (Δ*A*), cross section difference of first and last echoes (ΔCS), time from first to last echoes (Δ*t*), overlap area of first and second echoes (OA), overlap width of first and second echoes (OW). Besides, we also derived the spatial information on both single-echo and multi-echo features represented as the average and standard deviation of the waveform features from a cylindrical neighborhood (radius is 4 m) of each waveform. The cylindrical radius was selected based on half length of the smallest building in the area.

Feature selection

Not all the features are used for classification. Features are analyzed firstly and then major features are chosen for classification. In this study, major features were selected using Bhattacharyya distance (see Eq. (1)), which is applied successfully in research involving feature selection and extraction (Choi and Lee, 2003; Wang et al., 2014). The Bhattacharyya distance B_{ij} (Choi and Lee, 2003) has been used as a measure of the class separability of two land-cover types *i* and *j* for feature selection.

$$B_{ij} = \frac{1}{8}(M_i - M_j)^T \left(\frac{c_i + c_j}{2}\right)^{-1} (M_i - M_j) + \frac{1}{2} \ln \left[\frac{|(c_i + c_j)/2|}{(|c_i| \cdot |c_j|)^{1/2}} \right] \quad (1)$$

where M_i and C_j are the mean vector and covariance matrix of class *i*, respectively.

Classification models

Three classification models (model 1, model 2 and model 3) are set up for comparison in this study. The model 1 is the conventional echo-based classifier which utilizes a single classifier. The inputs for the classifier of model 1 are echo-based features since the original waveforms can be decomposed into individual echoes. The model 2 and model 3 are our proposed waveform-based models which combine two classifiers: a single-echo classifier and a multi-echo classifier. The two models utilize the single-echo features and multi-echo features for their inputs. The major features selected for inputs in the three models used in this study are shown in Table 3. In model 1, major features are amplitude, echo width, echo area, and cross section. In model 2 and 3, the selected major features were a combination of single-echo features and multi-echo features. The difference between model 2 and 3 is that model 3 additionally considers the optical features (R, G, and B). The RGB pixel values were exacted based on the nearest locations of single/first-echo LiDAR points.

Support vector machines (SVMs) were used as supervised learning algorithms, developed applying the associated statistical learning theory, to determine the optimal separation of classes (Vapnik, 1995). SVM can map non-linearly separable data onto a high dimensional space where the data can be separated linearly. SVM is used to identify the separating hyperplane that maximizes the distance between the closest training samples for any two classes. For high-dimensional classification problems, identifying a separating hyperplane in the feature space induced by the kernel function permits all computations to be performed in the original space (Vapnik, 1995). In this study, radial basis function (RBF) kernel was used in SVM, The implementation of multi-class SVM algorithm is achieved by using Matlab 2012a.Based on waveform

Table 3
Model input feature sets in the three point cloud classification models.

	Input features	
Model 1[a]		Am, *W*, *A*, CS
Model 2[a]	Single-echo classifier	Avg NR, Am, *W*, *A*, CS
	Multi-echo classifier	Avg NR, Avg *W*, Avg Δ*t*, Std ΔAm, Std Δ*W*, Std Δ*A*, Std CS, Std ΔCS, Std OW
Model 3[a]	Single-echo classifier	Avg NR, Am, *W*, *A*, CS, R, G, B[b]
	Multi-echo classifier	Avg NR, Avg *W*, Avg Δ*t*, Std ΔAm, Std Δ*W*, Std Δ*A*, Std CS, Std ΔCS, Std OW, R, G, B

[a] Model 1: echo-based classifier; Model 2 and 3: waveform-based classifiers.
[b] R, G, B: optical features from orthoimages.

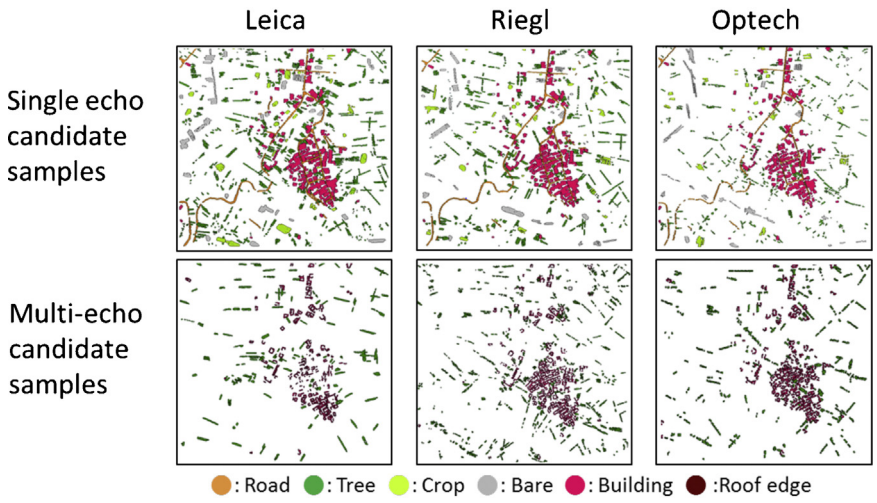

Fig. 3. Location of single-echo and multi-echo candidate samples in three LiDAR systems.

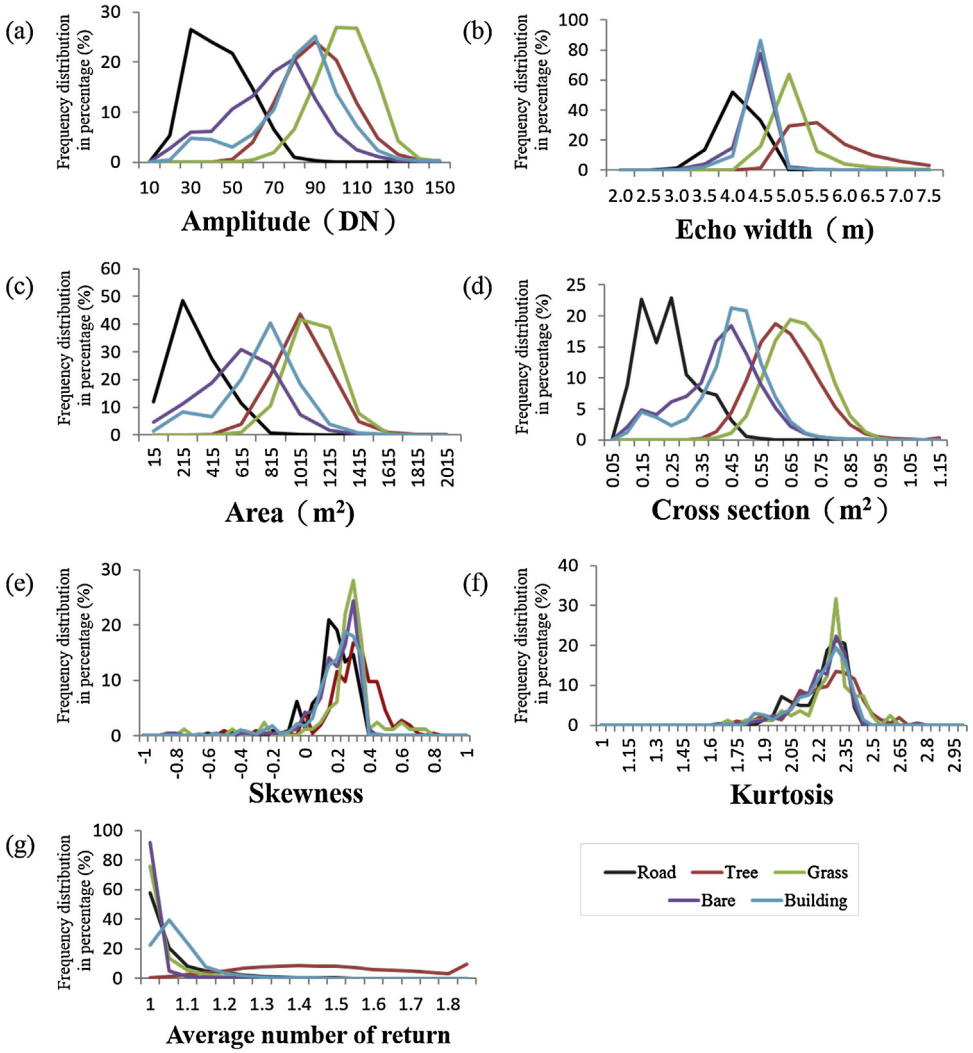

Fig. 4. Frequency distribution of full-waveform LiDAR features under various land cover: (a) amplitude, (b) echo width, (c) echo area, (d) cross section, (e) skewness, (f) kurtosis, and (g) average number of echoes.

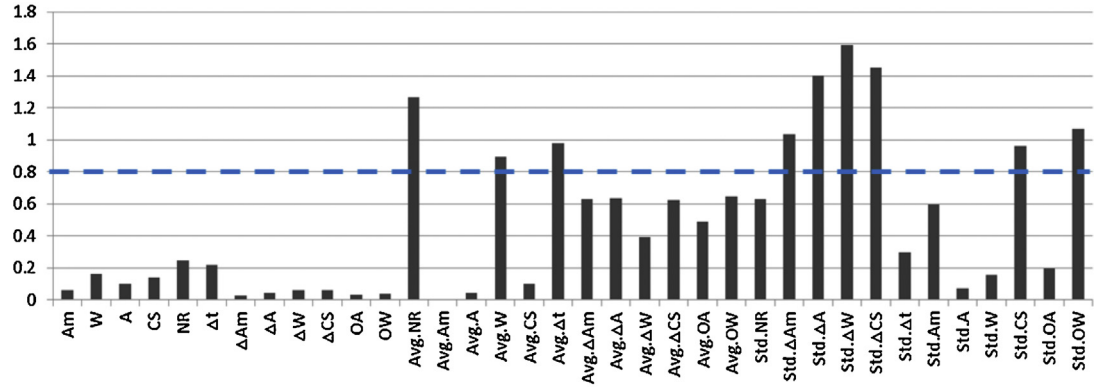

Fig. 5. Bhattacharyya distance between trees and roof edges for multi-echo waveform feature selection using the criterion i.e. Bhattacharyya distance is 0.8.

Table 4
Number of candidate samples with single-echo and multi-echo features under various land cover types in three LiDAR systems.

		Number of candidate samples		
		Leica	Riegl	Optech
Single-echo	Road	32,286	16,214	7061
	Tree	67,733	42,590	10,936
	Grass	37,762	15,058	7537
	Bare	46,485	18,765	9209
	Building	120,570	78,402	37,084
Multi-echo	Tree	37099	29016	12905
	Building roof edge	15165	12577	4466

features, the LiDAR points were classified into five major land-cover types: roads, trees (canopy), grass (grass and crop), bare (bare ground), and buildings (buildings and roof edges). Fig. 3 and Table 4 show the location and number of candidate sample points in the LiDAR systems. In each system, training points were randomly determined from 1% of the candidate sample points (Fig. 3). After training, the validation data were all candidate sample points except the training points. Both of the training and validation data were recognized and selected by using the TerraSolid's TerraScan.

Result and discussion

Fig. 4 shows the frequency percentage of single-echo features, such as echo amplitude, width, cross section and etc. in various land cover types. Echo amplitudes of single echoes were the highest for grass and lowest for roads in the study area (Fig. 4(a)). Echo width was generally wider for grass and trees than for buildings and roads (Fig. 4(b)), which agrees with previous results (Guo et al., 2011) indicating that wide echoes correspond to vegetation because vegetation spreads the LiDAR echoes, and that a narrow echo is likely to correspond to ground and buildings. The usefulness of echo cross section for classifying land cover and usage has been demonstrated before (Alexander et al., 2010). As shown in Fig. 4(c) and (d), echo area and cross section were high for vegetation, medium for buildings and bare ground, and low for roads. Thus, vegetation and non-vegetation can be identified based on echo cross section. In addition, the enhanced echo cross section based on incidence angle estimation will be considered to provide the radiometric information instead of delivering the information from orthoimages in the future (Abed et al., 2012; Abed, 2013). The distributions of skewness and kurtosis in echo amplitudes for various land-cover types are shown in Fig. 4(e) and (f). Skewness represents the degree of asymmetry around the mean, and kurtosis reflects the degree of peakedness in the distributions. The cases showing positive-skew indicate the tail on the right side of the LiDAR data. Because the kurtosis is less than 3, the distribution is more flattened than the normal distribution. However, skewness and kurtosis in echo amplitudes are not used as the major features for land cover classification. Fig. 4(g) shows the average number of echoes around cylindrical neighborhoods in various land-cover types. One can see that the trees contain the largest average number of echoes and second ones are buildings. The road, grass and bare earth contain the average number of echoes approach to 1. The average number of echoes is a major feature for distinguishing trees and buildings to other land cover types. From this test, the major single-echo based features were selected as average number of echoes, amplitude, echo width, echo area and cross section (model 1 in Table 3).

Most land-cover types except trees and roof edges presented only one major echo (single return), whereas the data in trees and

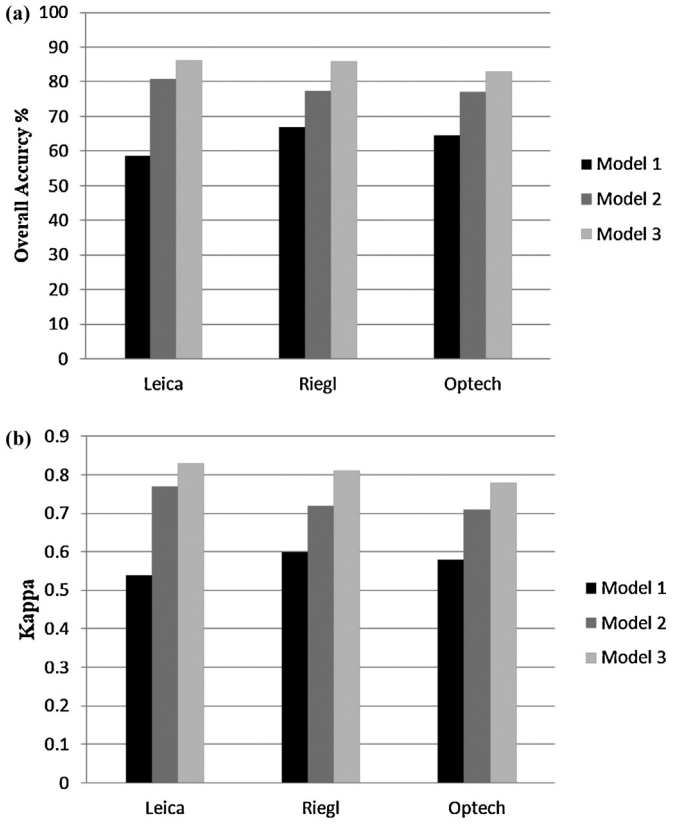

Fig. 6. (a) Overall accuracy and (b) Kappa of the three models for Leica, Riegl and Optech systems.

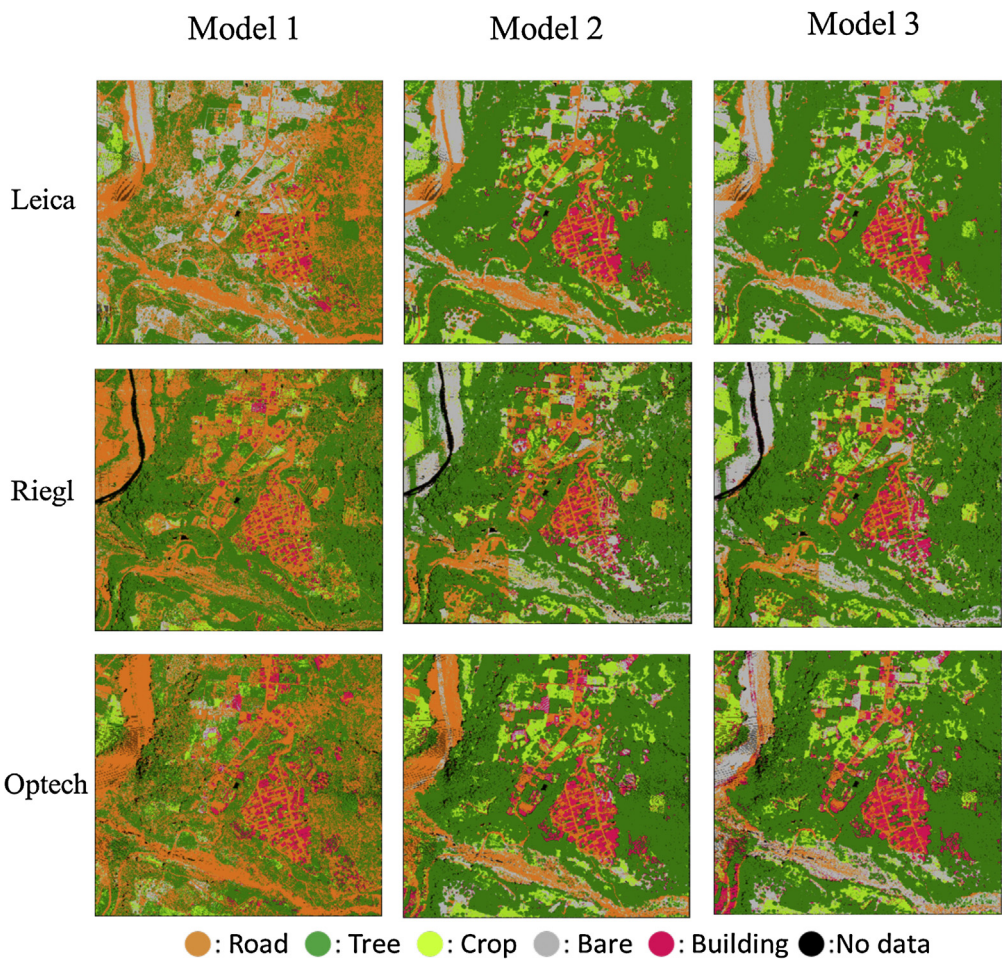

Fig. 7. Spatial pattern of point classification results in the three models for Leica, Riegl and Optech systems.

roof edges contained multi-echo waveform features. Thus, trees and roof edges could be identified readily when considering the number of echoes in the LiDAR waveform data. According to the relationship between classification error and the Bhattacharyya distance in (Choi and Lee, 2003), the criterion of Bhattacharyya distance is 0.8 if the nominal classification accuracy reaches 90%. Fig. 5 shows the Bhattacharyya distance measurements between trees and roof edges in multi-echo waveform features. The dominant features were selected based on this criterion (i.e., Bhattacharyya distance = 0.8). Thus, the dominant features for classifying land cover were Avg NR, Avg W, Avg Δt, Std ΔAm, Std ΔW, Std ΔA, Std CS, Std ΔCS, and Std OW, and these dominant features were selected for the multi-echo classifiers used in models 2 and 3. Our results also implied that the dominant features contained the spatial information of waveform features such as the average and standard derivation of the features around neighborhoods. However, the skewness and kurtosis of waveform data were not dominant features for classification in the study.

All nine confusion matrices from various models and LiDAR systems were listed in Appendix. Fig. 6 shows the overall accuracy

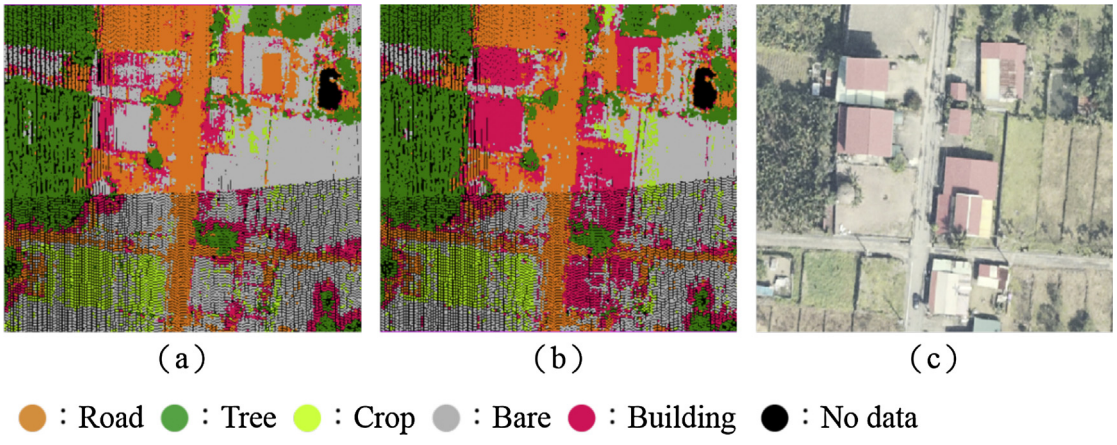

Fig. 8. Comparisons with detailed results in model 2 (a), model 3 (b), and orthoimage (c).

and Kappa of classification using the three models with data from the three LiDAR systems (Leica, Riegl, and Optech). These results are generally consistent in identifying waveform-based classifiers as being most accurate method in the various LiDAR systems. For example, in the Leica data, overall accuracies were 58.6%, 80.7%, and 86.0% and Kappa values were 0.54, 0.77, and 0.83 in model 1, model 2, and model 3, respectively. Comparing all results (Fig. 6) showed that model 3 classified land cover most accurately when both optical information and LiDAR waveform information were considered. Using image and LIDAR together enables more accurate vegetation classification than using the data independently (Ke et al., 2010). The full-waveform LiDAR system acquires waveform information about the land surface that represents the vertical nature of land cover, whereas optical images provide spectral information and can be used for classifying land cover. Therefore, in this study, LiDAR waveform and image data were integrated in model 3 for classifying land cover. Fig. 7 shows the spatial pattern of land-cover classifications in the three models based on the Leica, Riegl and Optech systems. In model 1, many bare ground and grass points were misclassified into road and tree, respectively. Model 2 can improve the classification that the more grass points were correctly classified into tree. However, grass points were more easily misclassified into road using Riegl system when compared with using Optech and Leica systems in Model 2. The poor discrimination between grass and road was found based on the amplitude information from Riegl system (Wang et al., 2014). Moreover, the most large classification errors happened between road and bare ground. A possible reason is that for the road and bare ground, the frequency distributions of all the waveform features are mostly overlapping in Fig. 4. Compared to three sensors in model 3 (Tables A.3, A.6 and A.9), bare ground was more seriously misclassified into road is in Optech and Leica than that in Riegl.

Model 2 based on waveform-based classifiers fits the data considerably better than model 1 using an echo-based classifier. However, without waveform-based classifiers in model 1, “tree” and “bare ground” were easily misclassified as “road” when compared to model 2 and 3. Table 5 presents user’s accuracy and producer’s accuracy in land-cover classification based on the Leica system. User’s accuracy is the probability that a sample from the classified data represents the same category on the ground. Generally, user’s accuracy was higher with model 2 than with model 1 (Table 5). The classification accuracy for roads was the lowest in model 1 because roads, buildings, and bare ground are land-cover types with similar textures, buildings and bare ground were misclassified as roads. User’s accuracy was greater overall with model 3 than with using model 2, although user’s accuracy for trees was slightly lower. User’s accuracy for bare ground was considerably higher with model 3 than with model 2. Moreover, producer’s accuracy is the probability that all the ground truth-points surveyed are classified under the same land-cover class by the producer of the map. Producer’s accuracy was greater with model 2 than with model 1 for most land-cover types except road, and the accuracy was greater with model 3 than with model 2 for grass, bare ground, and buildings. Collectively, our results

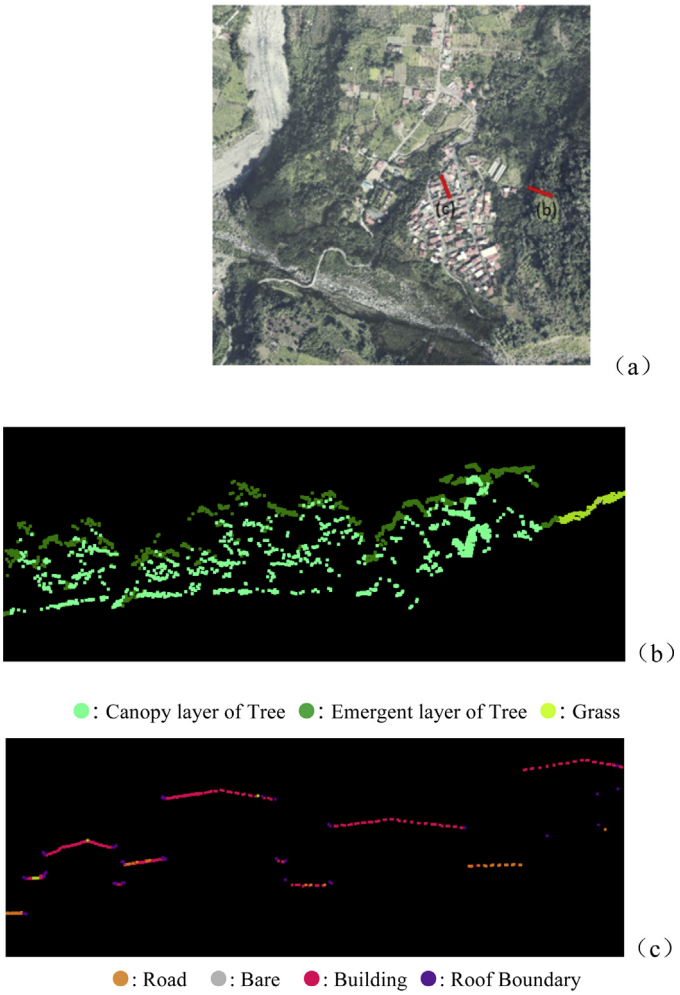

Fig. 9. (a) Location of cross-section profiles b and c. Cross-sectional classified LiDAR points in profile b for trees (b) and profile c for building roofs (c).

show that land-cover classification accuracy for trees and grass was greatest using model 3, which improved producer’s accuracy by 11% in building and reduced the misclassification of bare ground as buildings (Table 5). Generally, considering model 3, the misclassification of the buildings can be improved. The buildings can be separated from bare ground using additional optical image (RGB) information (Fig. 8). However, the producer’s accuracy for bare ground is still low and can be improved, because bare ground was often misclassified as buildings and roads. In future studies, we will consider further the detailed features that help distinguish roads, bare ground, and buildings reliably.

Traditionally, land cover has been classified in 2D based on image information, but 3D classification is feasible using LiDAR data. Fig. 9 shows the cross-section profiles of classified LiDAR point clouds around trees and building roofs. These results imply

Table 5
User’s and producer’s accuracy for various land cover types in the three models based on Leica system.[a]

	(%)	Road	Tree	Grass	Bare	Building
Model 1	User’s accuracy	29.3	78.8	47.1	34.7	92.1
	Producer’s accuracy	96.0	79.8	37.5	40.5	40.9
Model 2	User’s accuracy	46.9	95.5	82.5	64.6	95.1
	Producer’s accuracy	95.0	97.8	87.8	59.0	69.9
Model 3	User’s accuracy	52.1	95.2	88.6	81.5	96.5
	Producer’s accuracy	93.4	97.8	89.4	67.3	81.0

[a] Only from Leica system in the table. The confusion matrices of models based on three systems were listed in Appendix.

that land cover types can be well classified using full-waveform LiDAR data. For example, the canopy and roof edges can be effectively classified by the proposed classification model (Fig. 9(b) and (c)). For urban planning, building detection and change-type determination via LiDAR data analysis will be effective (Teo and Shih, 2012; Liu et al., 2013). For regional forest management, identifying vegetation species, vertical forest structure and inventory at landscape scales from LiDAR waveform data will be extremely useful (Nordkvist et al., 2011; Zimble et al., 2003; Palenichka et al., 2013; Hyyppä et al., 2008; Dinuls et al., 2012). Future study will consider full-waveform LiDAR data and high spatial resolution multispectral image for classification of individual trees into species. Fine spatial resolution DSM obtained via LiDAR data can be provided to analyze individual tree crowns in mixed forests.

Conclusions

The study integrated LiDAR waveform data, orthoimage data, and the spatial features of waveform data that can be used successfully in land-cover point cloud classification. Full-waveform LiDAR data offer advantages including the ability to consider 3D structures when classifying land cover. Compared to echo-based classifiers, waveform-based classifiers were used to effectively identify various land-cover types along the path of a laser pulse. Waveform-based classifiers can improve the poor performance (e.g., grass points were misclassified into trees).

Results obtained using data from LiDAR systems with Leica, Riegl, and Optech sensors showed that major land covers were classified consistently in this study, indicating that waveform-based classifiers are suitable for analyzing LiDAR waveform data for various land-cover types when compared to the echo-based classifier. Moreover, our results showed that land cover can be classified more accurately by using both LiDAR and image data than by using LiDAR data alone. Full-waveform LiDAR data acquires waveform information about the land surface that represents vertical structures in land cover, whereas optical images provide spectral information that facilitates land-cover classification. The model proposed in this study can provide land use planners with information combining distinct types of Full-waveform LiDAR and orthoimage data that can help in classifying land cover accurately based on waveform-based classifiers.

Acknowledgement

The authors wish to thank the editors and reviewers for their valuable comments and suggestions. This research was supported by a grant from the National Science Council, R.O.C. (NSC-101-2221-E-006-181-MY3).

Appendix.

Table A.1
Confusion matrix using classification model 1 in Leica system.

	Number of samples		Predictions (%)				
			Road	Tree	Grass	Bare	Building
Observations	32,286	Road	96.04	0.75	0.11	2.59	0.51
	133,967	Tree	14.69	79.83	2.87	1.59	1.01
	37,762	Grass	0.21	57.48	37.47	2.79	2.06
	46,485	Bare	43.98	3.04	7.25	40.45	5.28
	135,735	Building	25.58	3.96	6.38	23.17	40.91
		Overall accuracy (%): 58.63					
		Kappa: 0.54					

Table A.2
Confusion matrix using classification model 2 in Leica system.

	Number of samples		Predictions (%)				
			Road	Tree	Grass	Bare	Building
Observations	32,286	Road	94.96	0.14	0.07	2.25	2.58
	96,868	Tree	0.07	97.88	0.94	0.05	1.06
	37,762	Grass	0.10	8.12	87.77	1.13	2.87
	46,485	Bare	29.82	0.42	7.20	58.96	3.59
	128,068	Building	16.25	0.91	2.14	10.82	69.89
		Overall accuracy (%): 80.69					
		Kappa: 0.77					

Table A.3
Confusion matrix using classification model 3 in Leica system.

	Number of samples		Predictions (%)				
			Road	Tree	Grass	Bare	Building
Observations	32,286	Road	93.37	0.13	0.13	3.22	3.14
	96,868	Tree	0.06	97.75	0.99	0.06	1.14
	37,762	Grass	0.24	8.42	89.44	0.68	1.22
	46,485	Bare	24.85	0.38	4.77	67.31	2.69
	128,068	Building	12.52	1.07	0.87	4.49	81.04
		Overall accuracy (%): 86.01					
		Kappa: 0.83					

Table A.4
Confusion matrix using classification model 1 in Riegl system.

	Number of samples		Predictions (%)				
			Road	Tree	Grass	Bare	Building
Observations	16,214	Road	94.68	1.70	1.02	0.25	2.34
	71,606	Tree	6.96	91.18	1.32	0.27	0.28
	15,058	Grass	26.99	27.45	39.61	0.83	5.12
	18,765	Bare	52.73	18.58	15.32	3.65	9.73
	90,979	Building	25.05	7.37	6.91	0.34	60.33
		Overall accuracy (%): 66.87 Kappa: 0.60					

Table A.5
Confusion matrix using classification model 2 in Riegl system.

	Number of samples		Predictions (%)				
			Road	Tree	Grass	Bare	Building
Observations	16,214	Road	88.07	1.11	2.28	4.99	3.55
	56,620	Tree	2.41	94.62	0.53	0.68	1.76
	15,058	Grass	10.79	7.17	73.46	3.08	5.49
	18,765	Bare	19.28	5.05	29.59	42.25	3.84
	84,609	Building	14.39	2.27	4.20	6.68	72.46
		Overall accuracy (%): 77.41 Kappa: 0.72					

Table A.6
Confusion matrix using classification model 3 in Riegl system.

	Number of samples		Predictions (%)				
			Road	Tree	Grass	Bare	Building
Observations	16,214	Road	85.17	2.17	1.60	4.98	6.07
	56,620	Tree	1.27	94.82	0.53	0.35	3.03
	15,058	Grass	2.31	6.02	83.02	3.45	5.21
	18,765	Bare	13.31	3.07	12.37	65.98	5.27
	84,609	Building	8.90	1.78	1.33	3.31	84.68
		Overall accuracy (%): 85.76 Kappa: 0.81					

Table A.7
Confusion matrix using classification model 1 in Optech system.

	Number of samples		Predictions (%)				
			Road	Tree	Grass	Bare	Building
Observations	7061	Road	98.41	0.17	0.13	0.28	1.01
	23,841	Tree	20.47	70.47	3.31	0.31	5.44
	7537	Grass	0.37	45.97	50.98	0.61	2.07
	9209	Bare	70.75	7.84	9.87	1.53	10.01
	41,550	Building	21.50	2.29	3.56	0.88	71.76
		Overall accuracy (%): 64.52 Kappa: 0.58					

Table A.8
Confusion matrix using classification model 2 in Optech system.

	Number of samples		Predictions (%)				
			Road	Tree	Grass	Bare	Building
Observations	7061	Road	94.25	2.21	0.07	1.16	2.31
	16,915	Tree	0.53	94.98	1.47	0.15	2.87
	7537	Grass	0.34	4.96	88.56	2.79	3.34
	9209	Bare	67.79	0.12	13.02	13.33	5.73
	39,303	Building	13.47	0.86	2.05	4.38	79.24
		Overall accuracy (%): 77.18 Kappa: 0.71					

Table A.9
Confusion matrix using classification model 3 in Optech system.

Number of samples			Predictions (%)				
			Road	Tree	Grass	Bare	Building
Observations	7061	Road	83.05	0.62	0.00	6.34	9.98
	16,915	Tree	0.27	93.08	1.63	0.11	4.91
	7537	Grass	0.03	4.43	86.28	2.27	6.99
	9209	Bare	35.24	0.12	9.05	49.05	6.55
	39,303	Building	10.38	1.01	1.04	1.95	85.61
			Overall accuracy (%): 82.82 Kappa: 0.78				

References

Abed, F.M., 2013. Potential of the incidence angle effect on the radiometric calibration of full-waveform airborne laser scanning in urban areas. Am. J. Remote Sens. 1, 77–87.

Abed, F.M., Mills, J.P., Miller, P.E., 2012. Calibration of full-waveform ALS data based on robust incidence angle estimation. In: Int. Arch. Photogramm. Remote Sens. Spatial Inf. Sci., XXXVIII-5/W12, pp. 25–30.

Alexander, C., Tansey, K., Kaduk, J., Holland, D., Tate, N.J., 2010. Backscatter coefficient as an attribute for the classification of full-waveform airborne laser scanning data in urban areas. ISPRS J. Photogramm. Remote Sens. 65, 423–432.

Choi, E., Lee, C., 2003. Feature extraction based on the Bhattacharyya distance. Pattern Recognit. 36, 1703–1709.

Crosilla, F., Macorig, D., Scaioni, M., Sebastianutti, I., Visintini, D., 2013. LiDAR data filtering and classification by skewness and kurtosis iterative analysis of multiple point cloud data categories. Appl. Geomat. 5, 225–240.

Dalponte, M., Bruzzone, L., Gianelle, D., 2008. Fusion of hyperspectral and LIDAR remote sensing data for classification of complex forest areas. IEEE Trans. Geosci. Remote Sens. 46, 1416–1427.

Dinuls, R., Erins, G., Lorencs, A., Mednieks, I., Sinica-Sinavskis, J., 2012. Tree species identification in mixed Baltic forest using LiDAR and multispectral data. IEEE J. Sel. Topics Appl. Earth Observ. Remote Sens. 5, 594–603.

Guo, L., Chehata, N., Mallet, C., Boukir, S., 2011. Relevance of airborne lidar and multispectral image data for urban scene classification using random forests. ISPRS J. Photogramm. Remote Sens. 66, 56–66.

Höfle, B., Pfeifer, N., 2007. Correction of laser scanning intensity data: data and model-driven approaches. ISPRS J. Photogramm. Remote Sens. 62, 415–433.

Heinzel, J., Koch, B., 2011. Exploring full-waveform LiDAR parameters for tree species classification. Int. J. Appl. Earth Observ. Geoinf. 13, 152–160.

Hollaus, M., Aubrecht, C., Höfle, B., Steinnocher, K., Wagner, W., 2011. Roughness mapping on various vertical scales based on full-waveform airborne laser scanning data. Remote Sens. 3, 503–523.

Hyyppä, J., Hyyppä, H., Leckie, D., Gougeon, F., Yu, X., Maltamo, M., 2008. Review of methods of small-footprint airborne laser scanning for extracting forest inventory data in boreal forests. Int. J. Remote Sens. 29, 1339–1366.

Jutzi, B., Stilla, U., 2003. Laser pulse analysis for reconstruction and classification of urban objects. In: Int. Arch. Photogramm. Remote Sens, pp. 151–156.

Ke, Y., Quackenbush, L.J., Im, J., 2010. Synergistic use of QuickBird multispectral imagery and LIDAR data for object-based forest species classification. Remote Sens. Environ. 114, 1141–1154.

Liu, C., Shi, B., Yang, X., Li, N., Wu, H., 2013. Automatic buildings extraction from LiDAR data in urban area by neural oscillator network of visual cortex. IEEE J. Sel. Topics Appl. Earth Observ. Remote Sens. 6, 2008–2019.

Mallet, C., Bretar, F., Roux, M., Soergel, U., Heipke, C., 2011. Relevance assessment of full-waveform lidar data for urban area classification. ISPRS J. Photogramm. Remote Sens. 66, S71–S84.

Mutlu, M., Popescu, S.C., Stripling, C., Spencer, T., 2008. Mapping surface fuel models using lidar and multispectral data fusion for fire behavior. Remote Sens. Environ. 112, 274–285.

Nordkvist, K., Granholm, A.-H., Holmgren, J., Olsson, H., Nilsson, M., 2011. Combining optical satellite data and airborne laser scanner data for vegetation classification. Remote Sens. Lett. 3, 393–401.

Palenichka, R., Doyon, F., Lakhssassi, A., Zaremba, M.B., 2013. Multi-scale segmentation of forest areas and tree detection in LiDAR images by the attentive vision method. IEEE J. Sel. Topics Appl. Earth Observ. Remote Sens. 6, 1313–1323.

Teo, T.-A., Shih, T.-Y., 2012. Lidar-based change detection and change-type determination in urban areas. Int. J. Remote Sens. 34, 968–981.

Vapnik, V.N., 1995. The Nature of Statistical Learning Theory. Springer-Verlag, Inc., New York.

Wagner, W., Hollaus, M., Briese, C., Ducic, V., 2008. 3D vegetation mapping using small-footprint full-waveform airborne laser scanners. Int. J. Remote Sens. 29, 1433–1452.

Wagner, W., Ullrich, A., Ducic, V., Melzer, T., Studnicka, N., 2006. Gaussian decomposition and calibration of a novel small-footprint full-waveform digitising airborne laser scanner. ISPRS J. Photogramm. Remote Sens. 60, 100–112.

Wang, C.K., 2012. Exploring weak and overlapped returns of a lidar waveform with a wavelet-based echo detector. In: Int. Arch. Photogramm. Remote Sens. Spatial Inf. Sci., XXXIX-B7, pp. 529–534.

Wang, C.K., Tseng, Y.H., Chu, H.J., 2014. Airborne dual-wavelength LiDAR data for classifying land cover. Remote Sens. 6 (1), 700–715.

Zimble, D.A., Evans, D.L., Carlson, G.C., Parker, R.C., Grado, S.C., Gerard, P.D., 2003. Characterizing vertical forest structure using small-footprint airborne LiDAR. Remote Sens. Environ. 87, 171–182.